Letters on materials 7 (4), 2017 pp. 407-411 www.lettersonmaterials.com

DOI: 10.22226/2410-3535-2017-4-407-411 PACS 81.05.Je, 87.15.La

Predicting the mechanical properties of ultra-high temperature ceramics

V. V. Skripnyak†, V. A. Skripnyak

†skrp2012@yandex.ru

National Research Tomsk State University, Lenin Avenue 36, Tomsk, 634050, Russia

A model for predicting mechanical properties of ultra-high temperature ceramics (UHTC) and composites within a wide temperature range is presented. The model can be useful for predicting the mechanical properties of UHTC composites under dynamic loading and thermal shock. Results of calculations taking into account the dependences of the nonlinearity of normalized elastic moduli on the homologous temperature in the range $T/T_m = 0.2 – 0.62$ are presented.. Residual stresses in ZrB_2 composites reinforced with particles of refractory borides, carbides and nitrides after selective laser sintering (SLS) or spark plasma sintering (SPS) are predicted. It is shown that the fracture toughness K_{IC} of UHTC increases at the sintering temperature in the range $(0.45 – 0.62)\ T_m$. The residual stress in the matrix of ceramic composites can be either negative or positive due to a difference between the thermal expansion coefficients of the matrix and inclusion phases. It is shown that the fracture toughness and the flexural strength of ZrB_2 matrix composites can be increased by 25% by the introduction of inclusions of specially selected refractory strengthening phases. Dependence of the normalized strength of composites ZrB_2-B_4C on the logarithm of normalized strain rate can be described by a power law in the range of strain rates from 10^{-3} to 10^6 s^{-1} and temperatures from 295 K to about 1673 K. Results of simulations confirm that the technologies of SLS and SPS can be used for the production of UHTC composites with high values of the specific strength and the fracture toughness.

Keywords: flexural strength, fracture toughness, UHTC.

1. Introduction

There is a great interest to the processing of ultra-high temperature ceramics (UHTCs) by additive manufacturing (AM) technologies. These materials possess a high oxidation and thermal shock resistance and are used in a wide variety of structural applications, including nozzles, leading edges and nose caps of space vehicles re-entering the earth's atmosphere, cutting tools, bearings, igniters, and others.

The list of UHTC materials with melting temperatures above 3000 K is limited to perhaps 16 phases or compounds (Table 1). Among these UHTCs, ZrB_2 ceramic composites are the most promising for high temperature application due to their good combination high-temperature mechanical properties, resistance to oxidation, good electrical conductivity and the lowest theoretical density [1]. In recent years, the processes of additive manufacturing including selective laser sintering (SLS) and spark plasma sintering (SPS) have been used for the production of ceramic structural elements [2 – 9]. SLS is an additive manufacturing process for creating 3D parts with complex geometries because the use of powder bed SPS makes it possible to densify the UHTC composites at a lower temperature and in a shorter time as compared to conventional techniques of hot isostatic pressing (HIP). The use of SLS and SPS allows creating new composite materials simultaneously with the manufacture of structural elements.

The main problem in creating high strength UHTCs is connected with difficulties of consolidation due to high melting point and low self-diffusion coefficient of borides, carbides, and nitrides phases.

Recently, Yadhukulakrishnan [5] reported on a processing of UHTC zirconium diboride matrix composites reinforced by silicon carbides and multi-walled carbon nanotubes by using the SPS method at 2200 K. The porosity of ceramic composites ranged from 15% to almost zero. Zapata-Solvas [6] showed that the use of SPS allowed processing of ZrB_2-SiC and HfB_2-SiC composites with higher values of hardness, flexural strength and fracture toughness at room temperature, at 1700 K and 2100 K in comparison with analogs obtained by the HIP fabrication method. For the ZrB_2-SiC system the flexural strength is increased by addition of second phases such as SiC and La_2O_3, from 450 to ~700 MPa and from 500 to ~700 MPa in HfB_2-based UHTCs. Hu [7] found that (Zr,Ti)B_2-(Zr,Ti)N composites could be manufactured at 1900 – 2200 K by SPS using ZrB_2 and TiN powders. Guo [8] manufactured the ZrB_2-ZrC-SiC composites with AlN and Si_3N_4 additives and porosity from 15% to 0.1% by SPS method. The possibility of changing the values of Young's modulus and the shear modulus of the composites twice was discovered.

The elastic properties are important mechanical properties of UHTCs for structural design and they are closely linked with the composition, microstructure and additives. Therefore, it is important to study the mechanical properties of UHTC materials created by AM technologies and the effects of phase additives and porosity on these properties. In present study, this approach was used to develop a two-scale model.

2. Materials and methods

Young's modulus of solid phases is determined principally by interatomic forces, which decrease sharply with the interatomic distance in crystalline lattice (Table 1).

Young's modulus and shear modulus of fully densified UHTC composites can be described by the mixture rule and for porous media the values are decreased [10].

The theoretical mass density of ceramic composites irrespective of the chemical or phase composition of the matrix or skeleton phase can be determined as

$$\rho_{theor} = \sum_{i=1}^{n} C_i \rho_i, \quad (1)$$

where ρ_{theor} is the theoretical mass density of composite material, C_i is the volume fractions of the i phases, ρ_i is the mass density of the i-phases, n is the number of phases in composite material.

Effective elastic moduli M_e (where M_e stands for the Young's modulus E, the shear modulus μ or the bulk modulus K, respectively, and the subscript "e", denotes "effective") of full dense ceramics are temperature-dependent and calculated using the following equation:

$$M_e^{theor} = \sum_{i=1}^{n} C_i M_i, \quad (2)$$

where C_i is the volume fractions of the i phase, M_i is the elastic modulus of the i-phase.

Relative elastic moduli of porous ceramics are determined by Eq. [10]:

$$\xi = M_e / M_e^{theor}, \quad (3)$$

where ξ is the relative elastic modulus, M_e is the effective elastic modulus of porous ceramics and M_e^{theor} is the elastic modulus (E and μ) of the composite materials or the elastic modulus of the solid skeleton-frame phase (in the case of open-pore cellular solid body or foams).

Relative elastic moduli ξ of porous ceramics can be calculated by Eq. [10]:

$$\xi = \exp\left(\frac{-bp}{1-p/p_{th}}\right), \quad (4)$$

where p is the specific volume of pores, p_{th} is the critical porosity at occurrence of a percolation threshold in a porous structure, and b is the fitting coefficient. At the assumption of isolated spherical pores we can set $b = 2$.

Pubst [10] assessed $b = 0.74 \pm 0.09$ for monolithic Al_2O_3, SiC, ZrO_2, Si_3N_4 ceramics with porosity below $p_{th} \sim 60\%$. The values of the parameter $b = 2.21$, and 7.78 were determined for ZrB_2 and SiC, respectively. At porosity less than 0.6 the relative elastic modulus ξ of porous ceramics can be calculated using the equation:

$$\xi = (1-p)[1-p/0.648], \quad (5)$$

The elastic modulus of UHTC composites can be predicted using Eq. (2), (3) and Eq. (5).

The microstructure of the nanocomposites is constructed by dispersing second-phase nano-size particles within the matrix grains and on the grain boundaries. The mismatch of thermal expansions between the matrix and inclusions is the cause of residual stresses in composites after cooling from sintering temperature to room temperature.

Modern SLS and SPS technologies use a sintering temperature from 1900 K to 2200 K for densification of UHTCs [1 – 8]. Residual stresses can be either tensile or compressiveand cause both reducing and increasing the flexural strength and fracture toughness of UHTC composites as compared to single-phase ceramic materials. Recently

Table 1. Mechanical and thermodynamic properties of UHTC [1 – 18].

Phase/crystalline lattice	ρ, 10^3 kg/m^3	E, GPa	ν	α, 10^{-6} K^{-1} in range (293 – 1300 K)	T_m, K	θ_D, K
HfB_2 / Hexagonal	11.19	530	0.12	6.3	3653	690
HfC / FCC	12.76	352 – 462	0.18	6.6	4173	680
HfN / FCC	13.9	380	0.25	6.5	3658	684
ZrB_2 / Hexagonal	6.10	450 – 500	0.128	5.9 – 6.5	3518	942
ZrC / FCC	6.56	348	0.18	6.7	3673	744
ZrN / FCC	7.29	510	0.25	6.7	3223	684
TiB_2 / Hexagonal	4.52	575	0.14	4.6 – 5.2	3498	820 – 1140
TiC / Cubic	4.94	460 – 497	0.19 – 0.25	7.95 – 8.58	3373	916
TiN / FCC	5.39	440 – 615	0.12	9.35	3223	809
TaB_2 / Hexagonal	12.54	551		8.2	3313	1309
TaC / Cubic	14.50	472	0.1719	6.3	4073	776
WC / Hexagonal	15.77	668 – 714	0.24	3.85 – 3.9	3143	779
TaN / Cubic	14.30	466	0.246	8.31	2973	
SiC / Polymorphic	3.21	454	0.16	4.7	3093	1200
B_4C / Rhombohedral	2.52	432 – 463	0.15 – 0.18	4.5	2718	1016
ZrO_2 / Polymorphic	6.05	360	0.303 – 0.312	8.0 – 10.6	2973	590
Al_2O_3 / Polymorphic	3.97	395.8	0.254	8.8	2303	1100
Si_3N_4 / Polymorphic	3.29	166 – 310	0.23 – 0.276	2.64 – 3.3	2661 – 2769	1178

Watts et al. [11] have determined tensile stresses of ~800 MPa in the ZrB_2 matrix of (ZrB_2 – 30% vol. SiC) ceramics using Raman spectroscopy and neutron diffraction methods.

The first invariant of the residual stress tensor can be estimated by formula [12]:

$$p_{res} = \frac{2(\alpha_m - \alpha_{inc})(T - T_r)E_m E_{inc}}{E_{inc}(1+\nu_m) + 2E_m(1-2\nu_{inc})}, \quad (6)$$

where p_{res} is the residual pressure, α_m, α_{inc} are the linear thermal expansion coefficients of matrix and inclusion, respectively, T, T_r are the sintering temperature, and the room temperature, E_m, E_{inc}, ν_m, ν_{inc} is Young's modulus and Poisson's ratio; subscripts m and inc correspond to matrix and inclusions, respectively.

In addition, the tensile stress decreases with the distance from the interface between grains of the matrix and the inclusion [12]

$$p_{res} = \frac{(\alpha_m - \alpha_{inc})(T - T_r)E_m E_{inc}}{E_{inc}(1-2\nu_m) + 2E_m(1-2\nu_{inc})}\left(\frac{d}{r+d}\right)^3, \quad (7)$$

where d, r are the size of the inclusion and the radial distance from the inclusion surface, respectively.

The linear thermal expansion coefficients of UHTCs within the temperature range from 295 K to 2200 K were described by phenomenological relation [4,18]:

$$\alpha(T) = \alpha_0 + \alpha_1 T + \alpha_2 T^2 + \alpha_3 T^3, \quad (8)$$

where α_0, α_1, α_2, α_3 are constants of material.

For calculation $\alpha(T)$ of ZrB_2, α_0, α_1, α_2, α_3 values of -1.64×10^{-3}, 4.92×10^{-6}, 1.72×10^{-9}, and -2.31×10^{-13}, respectively were used. Equation (8) to HfC, TaC, TiC, ZrC takes the form of a linear equation ($\alpha_2 = \alpha_3 = 0$) [18].

The increment of the fracture toughness K_{IC} due to residual stress can be estimated using the equation [13]:

$$\Delta K_{IC} = \frac{-2C_{inc}\, p_{res}}{1 - C_{inc}}\sqrt{\frac{2(L-d)}{\pi}}, \quad (9)$$

where C_{inc} is the volume fractions of inclusions, L is the average distance between inclusions, d is the average size of inclusions, p_{res} is the residual pressure in the matrix. The relationship between Young's modulus and temperature is assumed to satisfy the following relationship [14]:

$$E = E_0 - B_0 T\exp(-T_m/T) + \\ + B_1(T - B_2 T_m + |T - B_2 T_m|)\exp(-T_m/T), \quad (10)$$

where E_0 is Young's modulus at 273 K, Tm is the melting temperature of solid phase, and B_0, B_1, B_2 are material constants.

Eq. (10) can be simplified to the form of an empirical Wachtman equation [17]:

$$E = E_0 - B_0 T\exp(-\theta_D/2T), \quad (11)$$

where θ_D is the Debye temperature.

Eq. (11) can be used for calculating Young's modulus for UHTCs at temperatures below ~0.25 T_m (T_m is the melting temperature) [15 – 17].

Temperature dependence of Poisson's ratio can be described by the linear relationship (11):

$$\nu(T) = \nu_0 - k_\nu T, \quad (12)$$

where ν is Poisson's ratio, and ν_0, k_ν are constants of UHTC phases.

Temperature dependence of the shear modulus $\mu(T)$ and the bulk modulus $B(T)$ can be calculated using the equations:

$$\mu(T) = E(T)/2(1+\nu(T)), \\ B(T) = E(T)/3(1-2\nu(T)). \quad (13)$$

The temperature dependent the flexural strength $\sigma_f(T)$ of the UHTCs is described by Eq. [15]

$$\sigma_f(T) = \sqrt{\frac{(\sigma_f^0)^2}{E_0}E(T)\left[1 - \int_{273}^{T} C_p(T)\mathrm{d}t\right] \Big/ \int_{273}^{T} C_p(T)\mathrm{d}t},$$

where σ_f^0 is the fracture strength at the reference temperature, E_0 is Young's modulus at the reference temperature and $E(T)$ is the temperature-dependent Young's modulus, $C_p(T)$ is the specific heat capacity for constant pressure, and T_m is the melting temperature.

The temperature dependence of UHTC specific heat capacity C_p can be approximated by:

$$C_p(T) = c_0 + c_1 T + c_2 T^2, \quad (14)$$

where c_0, c_1, c_2 are constants of material, T is temperature.

For calculating $C_p(T)$ of ZrB_2, c_0, c_1, c_2 values of 15.34, 0.00225, and -3.96×10^5, respectively, were used.

The dependence of the dynamic compressive strength of ceramic materials at macro-scale level on the strain rates was described using dimensionless simplexes and complexes [8 – 10]:

$$\mu(T) = E(T)/2(1+\nu(T)), \\ B(T) = E(T)/3(1-2\nu(T)). \quad (15)$$

where σ_f/σ_0 is the normalized macroscopic thresholds stress of the ceramic under compression, $\dot{\varepsilon}_{eq}/\dot{\varepsilon}_0$ is the normalized strain rate, $\dot{\varepsilon}_{eq} = [(2/3)\dot{\varepsilon}_{ij}\dot{\varepsilon}_{ij}]^{1/2}$, η is a flaw density, a is a flaw radius, ρ is the effective mass density, $\dot{\varepsilon}$ is the strain rate, K_{IC} is the fracture toughness, E is the Young's modulus.

3. Results and discussion

Fig. 1 shows the temperature dependence of Poisson's ratio for ZrB_2, HfB_2, TiB_2. Eq. (12) was used for calculation. Experimental data are shown by symbols [16].

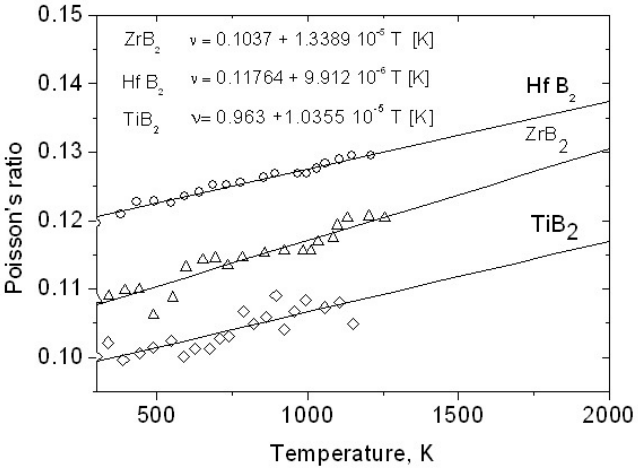

Fig. 1. Poisson's ratio of ZrB_2, HfB_2, TiB_2 vs temperature.

Fig. 2 shows the temperature dependence of the normalized Young's modulus of ZrB_2. The solid curve was calculated by Eq. (10) with coefficients $E_0 = 500$ GPa, $B_0 = 2.54$, $B_1 = 1.9$, $B_2 = 0.363$. The dashed curve was obtained by Eq. (10) with coefficients $E_0 = 500$ GPa, $B_0 = 1.2$, $B_1 = 0$, $B_2 = 0$. The experimental data are shown by symbols [17].

The Young's modulus decreases with increasing temperature. In almost all UHTC composites, the initial linear decrease, from room temperature up to about $\sim T_m/4$ (850 K for ZrB_2), is followed by another decrease with a steeper slope up to about $\sim 0.6\, T_m$ (2000 K for ZrB_2), after which the drop is much slower. Residual pressure depends on temperature drop and the difference between the thermal expansion coefficients of the matrix and inclusion phases. It is the difference in the coefficient of thermal expansion between ZrB_2 matrix and inclusions of UHTC phases. Thermo-mechanical properties of matrix and potential inclusions are given in Table 1. Upon cooling from the sintering temperatures, the SiC grains or the B_4C grains will not contract as quickly as the ZrB_2 matrix, resulting in a tensile residual stress in the ZrB_2 matrix. Calculated tensile stresses of ~800 MPa in the ZrB_2 matrix near SiC inclusions are in good agree with experimental data ~810 MPa for ZrB_2 – 30 vol. % SiC ceramics determined by using Raman spectroscopy and neutron diffraction methods [11]. Note the residual pressures in the matrix are both negative and positivein ZrB_2-TiC, ZrB_2-ZrO_2, ZrB_2-SiC, ZrB_2-B_4C composites. Due to the thermal expansion mismatch between ZrB_2 (5.9×10^{-6} K^{-1}) and (Hf,Ta)N, (Hf,Ta)B_2, (Hf,Ta)C, and ZrO_2, the residual tensile stresses may induce crack deflection along the grain boundaries, which contributes to the enhancement of fracture toughness. Increments of the fracture toughness KIC due to residual stress calculated using Eq. (9) are presented in Fig. 3.

The fracture toughness and the flexural strength of ZrB_2 ceramics sintered by the SPS method are ~3.6 MPa $m^{1/2}$, and 450 ± 40 MPa at room temperature, respectively [1]. These ceramics had a grain size of ~10 μm and porosity of ~2%. Composites ZrB_2-HfB_2, ZrB_2-HfC, ZrB_2-ZrC created by the SPS method may have 25% higher fracture toughness values, but slightly lower flexural strength, as can be seen from the results shown in Fig. 3. The calculated values of increments of the fracture toughness KIC for the composite materials ZrB_2-SiC, ZrB_2-ZrC, ZrB_2-TiB_2 when the volume concentration of inclusions are of 10 – 20% [1,4,13,19,20]. Note that the increment K_{IC} increases with increasing concentration of SiC up to 30%. The increase in K_{IC} was caused not only by the increase of the residual stress, but the increase in the fracture toughness due to reducing the size of the ZrB_2 grains in the ZrB_2-SiC composites obtained by SPS at sintering temperatures of ~2200 K. Sonber and co-authors [21] measured values of fracture toughness of ceramic composites ZrB_2-HfB_2. Fracture toughness K_{IC} of ZrB_2 – 10% HfB_2 – wt.% $TiSi_2$ was equal to 6.44 MPa $m^{1/2}$, and 6.59 MPa $m^{1/2}$ for ZrB_2 – 20% HfB_2– wt.% $TiSi_2$. Note, the coefficient of linear thermal expansion of $TiSi_2$ increases from –0.002 to +0.0136 K^{-1} in the temperature range from 293 K to 1800 K. The fracture toughness at room temperature decreased as compared to the composites without additives of metal silicides [1, 6, 21]. The calculated normalized compressive strength of ZrB_2-B_4C ceramics versus the logarithm of normalized strain rates are shown in Fig. 4.

Values of $a = 9.3$ μm, $\eta \approx 3.27\times10^{10}$ m^{-2} were used for calculation of the normalized compressive strength by Eq. (15).

Open symbols correspond to experimental data for ZrB_2 [1,22], the filled symbols are the data for ZrB_2 – 25% B_4C from [15]. Normalized strength at compression of ZrB_2 ceramics and composites ZrB_2-B_4C on the logarithm of normalized strain rate can be described by a power law in a wide range of strain rates. The dynamic strength of ZrB_2 ceramics decrease at a homologous temperature above $T/T_m > \sim 0.39$.

Results of simulation confirm that the technologies of SLS and SPS can be used for the production of UHTC based

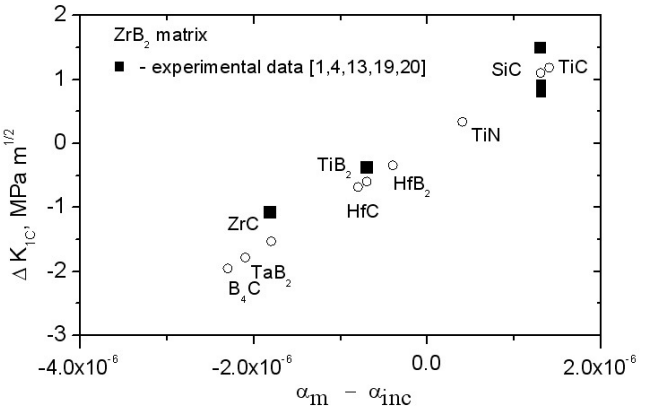

Fig. 3. Increment of the fracture toughness K_{IC} vs thermal expansion coefficients mismatch of matrix and inclusion.

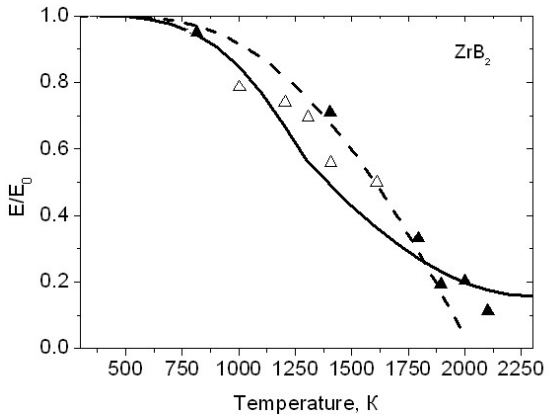

Fig. 2. Young's modulus of ZrB_2 vs temperature.

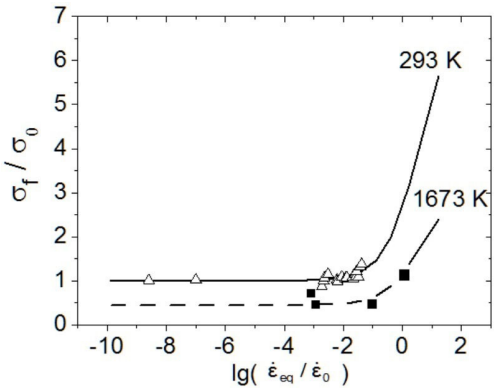

Fig. 4. Normalized fracture thresholds stress of ZrB_2 – 25 % B_4C versus the logarithm of normalized strain rates.

composites ZrB_2, TiB_2, SiC, B_4C, ZrC, TiC, and TiN, with high values of specific strength and fracture toughness. The computational model Eqs. (1) – (15) can be used for prediction of the mechanical properties of ceramic composites under quasi-static and dynamic compression in a wide temperature range. The model can be useful for predicting the mechanical properties of UHTC composites under dynamic loading and thermal shock.

4. Conclusions

A model is presented for predicting mechanical properties of ultra-high temperature ceramics (UHTCs) in a wide temperature range.

The relationship between Young's modulus and temperature of UHTC is nonlinear within homologous temperature range 0.45 – 0.62.

The fracture toughness of zirconium diboride matrix composites can be increased by 25% by the introduction of inclusions of specially selected refractory strengthening phases.

The residual pressures in the matrix of composites can be either negative or positive due to difference between the thermal expansion coefficients of the matrix and inclusion phases.

The normalized strength at compression of composites ZrB_2-B_4C on the logarithm of normalized strain rate can be described by a power law in the range of strain rates from 10^{-3} to 10^6 s^{-1} and temperatures from 295 K to ~1673 K.

Acknowledgments. This work was supported by the Russian Science Foundation (RSF), project no. 16-19-10264.

References

1. S.-Q. Guo, J. of Eur. Ceram. Soc., 29, 995 (2009). DOI: 10.1016/j.jeurceramsoc.2008.11.008
2. J. Deckers, J. Vleugels, J.-P. Kruth, J. Ceram. Sci. Tech., 5, 245 (2014). DOI: 10.4416/JCST2014-00032
3. S. Pattnaik, M. C. Leu, and G. E. Hilmas, J. of Virtual and Physical Prototyping, [cited 4 April 2015]. Available from: <http:// www.dtic.mil/cgi-bin/GetTRDoc?AD >.
4. Handbook of Ceramic Composites. Ed. by N. P. Bansal. Boston/Dordrecht/London. Kluwer Academic Publishers. 2005. 554 p. ISBN 1420 – 8133 – 2.
5. G. B. Yadhukulakrishnan, S. Karumuri, A. Rahman, et al., Ceram. Int., 39, 6637 (2013).
6. E. Zapata-Solvas, D. D. Jayaseelan, H. T. Lin, et al., J. Eur. Ceram. Soc., 33, 1373 (2013). DOI: 10.1016/j.jeurceramsoc.2012.12.009
7. C. Hu, Y. Sakka, H. Tanaka, et al., J. Alloys and Comp., 494, 266 (2010). DOI: 10.1016/j.jallcom.2010.01.006
8. S. Guo, Y. Kagawa, T. Nishimura, H. Tanaka, Ceram. Int., 34, 1811 (2008).
9. S. G. Huang, K. Vanmeensel, J. Vleugels, J. Eur. Ceram. Soc., 34, 1923 (2014). 10.1016/j.jeurceramsoc.2014.01.022
10. W. Pabst, E. Gregorova, G. Tich, J. Eur. Ceram. Soc, 26, 1085 (2006). DOI: 10.1016/j.jeurceramsoc.2005.01.041
11. J. Watts, G. E. Hilmas, W. G. Fahrenholtz, J Eur. Ceram. Soc., 30, 2165 (2010). DOI: 10.1016/j.jeurceramsoc.2010.02.014
12. J. W. Zimmermann, G. E. Hilmas, W. G. Fahrenholtz, Mater. Chem. Phys. 112, 140 (2008). DOI: 10.1016/j.matchemphys.2008.05.048
13. L. Silvestroni, D. Sciti, C. Melandri, S. Guicciardi, J. Eur. Ceram. Soc., 30, 2155 (2010). DOI: 10.1016/j.jeurceramsoc.2009.11.012
14. W. G. Li, R. Z. Wang, D. Y. Li, D. N. Fang, Phys. Res. Int., 2011, 1 (2011). DOI: 10.1155/2011/791545
15. W. G. Li, F. Yang, D. N. Fang, Acta Mech. Sinica, 26, 235 (2010). DOI: 10.1007/s10409-009-0326-7
16. D. E. Wiley, W. R. Manning, O. Hunter, JR., J. Less-Common Metalls, 18., 149 (1969).
17. S. Guicciardi, A. K. Swarnakar, O. Van der Biest et al., Scripta Mater. 62, 831 (2010). DOI: 10.1016/j.scriptamat.2010.02.011
18. S. Iikubo, H. Ohtani and M. Hasebe, Mater. Trans., 51, 574 (2010). DOI: 10.2320/matertrans.MBW200913
19. L. Rangaraj, S. J. Suresha, C. Divakar, and V. Jayaram, Metal. and mater. Trans. A, 39A, 831 (2008). DOI: 10.1007/s11661-008-9500-y
20. J. Yin, Z. Huanga, X. Liu et al., Mater. Sci. & Eng. A, 565, 414 (2013).
21. J. K. Sonber, T. S. R. Ch. Murthy, C. Subramanian, et al., Int. J. of Refr. Metal. and Hard Mater., 29, 21 (2011). DOI: 10.1016/j.ijrmhm.2010.06.007
22. I. K. Vaganova, V. A. Skripnyak, V. V. Skripnyak, E. G. Skripnyak, Appl. Mech. and Mater., 756 , 187(2015).